# Substrate-Specific Coupling of O₂ Activation to Hydroxylations of Aromatic Compounds by Rieske Non-heme Iron Dioxygenases

Sarah G. Pati,[§] Charlotte E. Bopp,[§] Hans-Peter E. Kohler, and Thomas B. Hofstetter*

Read Online

ACCESS | Metrics & More | Article Recommendations | Supporting Information

**ABSTRACT:** Rieske dioxygenases catalyze the initial steps in the hydroxylation of aromatic compounds and are critical for the metabolism of xenobiotic substances. Because substrates do not bind to the mononuclear non-heme $Fe^{II}$ center, elementary steps leading to O₂ activation and substrate hydroxylation are difficult to delineate, thus making it challenging to rationalize divergent observations on enzyme mechanisms, reactivity, and substrate specificity. Here, we show for nitrobenzene dioxygenase, a Rieske dioxygenase capable of transforming nitroarenes to nitrite and substituted catechols, that unproductive O₂ activation with the release of the unreacted substrate and reactive oxygen species represents an important path in the catalytic cycle. Through



correlation of O₂ uncoupling for a series of substituted nitroaromatic compounds with ¹⁸O and ¹³C kinetic isotope effects of dissolved O₂ and aromatic substrates, respectively, we show that O₂ uncoupling occurs after the rate-limiting formation of $Fe^{III}$-(hydro)peroxo species from which substrates are hydroxylated. Substituent effects on the extent of O₂ uncoupling suggest that the positioning of the substrate in the active site rather than the susceptibility of the substrate for attack by electrophilic oxygen species is responsible for unproductive O₂ uncoupling. The proposed catalytic cycle provides a mechanistic basis for assessing the very different efficiencies of substrate hydroxylation vs unproductive O₂ activation and generation of reactive oxygen species in reactions catalyzed by Rieske dioxygenases.

**KEYWORDS:** *non-heme ferrous iron oxygenases, nitrobenzene dioxygenase, biocatalysis, O₂ uncoupling, isotope effects, xenobiotics*
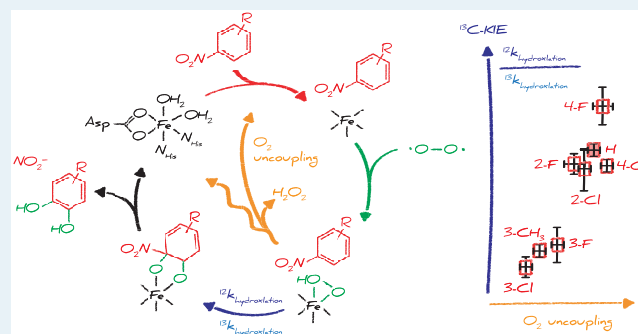
## INTRODUCTION

Rieske dioxygenases catalyze important hydroxylation, *O*-/*N*-dealkylation, and oxidative cyclization reactions in many catabolic and biosynthetic processes.[1−13] These enzymes belong to a subclass of mononuclear non-heme iron enzymes where O₂ is activated at an Fe center coordinated by two histidine and one carboxylate ligands.[14−26] Most oxygen-activating non-heme iron enzymes retrieve the four electrons for the reduction of O₂ from the substrate (extradiol-, intradiol-, and 2-hydroxyethylphosphonate dioxygenases)[27−33] or from a combination of substrates and cosubstrates (α-ketoglutarate- and pterin-dependent hydroxylases).[34,35] Rieske dioxygenases, in contrast, require the transfer of two electrons from the substrate and two additional electrons from NADH. These electrons are delivered through electron-transfer proteins to the Rieske cluster in the catalytically active oxygenase component. This oxygenase component consists of an $\alpha_3\beta_3$ trimer where each α-subunit contains a mononuclear non-heme $Fe^{II}$ and a [2Fe-2S] Rieske cluster.[36−40] Within the oxygenase, electrons are transferred to the non-heme Fe center in one α subunit from the Rieske cluster in the adjacent α subunit through the H-bond of an Asp residue at the subunit interface.[41] It is hypothesized that this

electron transfer is prerequisite for O₂ activation as it generates highly oxidized Fe-oxygen species. These species not only oxygenate a broad substrate spectrum of unactivated aromatic hydrocarbons but also highly electron-deficient nitrated and halogenated aromatic structures found in many persistent environmental contaminants.[39,40,42−44] Reactions of non-heme $Fe^{II}$ centers of Rieske dioxygenases are initiated through loss of a H₂O ligand, making the 5-coordinate $Fe^{II}$ site available for O₂ binding.[45,46] The presence of the substrate in the active site and a reduced Rieske cluster (i.e., its $Fe^{II}$-$Fe^{III}$-form) are both required for this change of $Fe^{II}$ coordination. However, the lack of substrate coordination at the $Fe^{II}$ center[37,47,48] makes it particularly difficult to identify reactive enzyme−substrate combinations as well as to delineate the sequence and energetics of the elementary reactions involved in O₂ activation

to Fe-oxygen species, Rieske cluster oxidation, and substrate hydroxylation.[46]

There are currently two hypotheses for the mechanism of dioxygenation by Rieske dioxygenases. Recent studies with benzoate dioxygenase (BZDO) suggest the formation of $Fe^{III}$-superoxo species after binding and one-electron reduction of $O_2$ by the non-heme $Fe^{II}$.[49−51] Attack of the $Fe^{III}$-superoxo species on the aromatic substrate generates a peroxo-bridged substrate radical in the rate-limiting step of the dioxygenation reaction. This step is followed by the fast proton-coupled electron transfer associated with Rieske cluster oxidation. The homolytic cleavage of the O−O bond in the $Fe^{III}$-peroxo bridge species gives rise to a substrate epoxide intermediate that will coordinate with the nonheme $Fe^{II}$ for the second oxygenation step.[50] This mechanism contrasts previous interpretations of data from naphthalene dioxygenases (NDO) where the two-electron reduction of bound $O_2$ with electrons from the non-heme $Fe^{II}$ and the reduced Rieske cluster results in $Fe^{III}$-peroxo and/or a putative $Fe^V$-oxo-hydroxo species.[45,52−55] Formation of these species including the O−O bond cleavage was found to proceed over higher barriers than the following substrate oxygenation steps.[50,56−58] As a consequence, a rate-limiting $O_2$ activation step without direct interactions between reactive Fe-oxygen species and the substrate needed to be postulated. These insights into the reactivity and mechanisms of Rieske dioxygenases originate largely from extensive spectroscopic, kinetic, and computational investigations of NDO[36,37,45,47,52,59,60] and BZDO[49,50,53,61] with their eponymous substrates, naphthalene and benzoate, respectively, as well as a few structurally related compounds used as mechanistic probes. The number of described substrates for NDO, BZDO, and other Rieske dioxygenases, especially those capable of transforming xenobiotic compounds in nature such as nitroarene and biphenyl dioxygenases, however, is large.[18,40,42,43,62−66] It remains an open question whether dioxygenations catalyzed by this family of enzymes share common reactive Fe-oxygen species and catalytic mechanisms. It is also unknown whether different substrates can modulate critical events in the catalytic cycle[67] in a way that might be interpreted as substrate-specific catalytic mechanisms.

Interestingly, discussions of Rieske dioxygenase reactivity rarely include quantitative considerations of the unproductive activation of $O_2$ without substrate metabolism. Rieske dioxygenases including naphthalene-, biphenyl-, and dibenzofuran dioxygenases show substantial $O_2$ consumption without concomitant formation of hydroxylated products.[65,66,68−71] This $O_2$ uncoupling not only gives rise to reduced substrate turnover but also to reactive oxygen species that can cause enzyme inactivation through hydroxylation of active site residues and mismetalation.[72−76] The phenomenon of $O_2$ uncoupling is reported prominently for $\alpha$-ketoglutarate-dependent non-heme $Fe^{II}$ oxygenases.[34,72−74,77−81] McCusker and Klinman[80,81] observed the uncoupling of substrate C−H hydroxylation from oxidative decarboxylation of the co-substrate ($\alpha$-ketoglutarate) due to subtle active-site perturbations affecting substrate positioning while the effect of substrates on $O_2$ binding and activation is maintained. No comparable evidence exists for the interpretation of substrate hydroxylation and $O_2$ uncoupling by Rieske dioxygenases. While the presence of the substrate in the active site is also a prerequisite for $O_2$ binding, it is unclear which active site properties and enzyme−substrate interactions cause loss of

activated $O_2$ as reactive oxygen species from Rieske dioxygenases. Evidence for oxidative stress related to the activity of Rieske dioxygenases[82−84] suggests that $O_2$ uncoupling may be an inherent element of the catalytic cycle.

Here, we evaluate the role of $O_2$ uncoupling in the catalytic cycle of Rieske dioxygenases and provide a mechanistic basis for assessing enzyme and substrate properties that can give rise to substrate hydroxylation vs unproductive $O_2$ activation and generation of reactive oxygen species. We focus our work on reactions of nitrobenzene dioxygenase (NBDO), a Rieske dioxygenase that, in addition to forming cis-dihydrodiols from (poly)aromatic hydrocarbons, catalyzes the dioxygenation of various nitroarenes to (substituted) catechols.[40] NBDO shares large sequence identity with NDO,[40] and the NBDO crystal structure (PDB-ID: 2BMQ[40]) also provided the basis for computational evaluations of the reactivity of $Fe^{III}$-superoxo vs $Fe^{III}$-peroxo species of BZDO.[50] In contrast to NDO and BZDO, nitroarene substrates of NBDO are hydrogen-bonded by an Asn residue in NBDO. This feature allows us to evaluate $O_2$ uncoupling systematically with a series of substituted nitrobenzenes assuming similar substrate alignment in the active site. We hypothesize that due to the absence of substrate interactions with the non-heme $Fe^{II}$ prior to $O_2$ activation, different substrates have minor impact on the type of activated Fe-oxygen species. To that end, we used competitive $^{18}O$ isotope effects of $O_2$ to probe for the timing of $O_2$ activation to reactive Fe-oxygen species.[85−89] On the other hand, $^{13}C$ substrate isotope effects were studied to evaluate the mechanism of aromatic substrate hydroxylation[90−92] and its timing in the catalytic cycle. Our data suggest that the release of unreacted substrate associated with $O_2$ uncoupling represents an important path in the catalytic cycle of Rieske dioxygenases that are often exposed to a broad substrate spectrum in nature.

## ■ EXPERIMENTAL SECTION

**Enzyme Assays.** All chemicals and enzymes used are reported in Section S1 of the Supporting Information (SI). Experimental procedures for enzyme assays with NBDO are described in detail by Pati et al.[90] and summarized below.

Experiments for the quantification of substrate turnover, product formation, and substrate and cosubstrate isotope effects were carried out in clear-glass crimp-top vials with butyl rubber stoppers and aluminum crimp seals. Vials were completely filled with 11 mL of aqueous solution. Assays consisted of 50 mM MES buffered at pH 6.8, 0.15 $\mu$M reductase, 1.8 $\mu$M ferredoxin, 0.15 $\mu$M oxygenase, 100 $\mu$M $(NH_4)_2Fe(SO_4)_2$, and 150−500 $\mu$M nitroaromatic substrate. Substrates were dissolved in MES buffer. All aqueous solutions were kept at 24−26 °C to establish initial dissolved $O_2$ concentrations of 240−260 $\mu$M. Reactions were initiated through addition of 50 to 300 $\mu$L of NADH stock solution (10−100 mM in 0.01 M NaOH) to closed reaction vessels with a gas-tight glass syringe. After complete NADH oxidation, vials were prepared for analysis of $^{18}O/^{16}O$ isotope ratios of dissolved $O_2$ as described previously.[90,93] Briefly, 3 mL of the assay solution was replaced with $N_2$ gas before reactors were placed upside down on an orbital shaker at 200 rpm for 30 min to facilitate partitioning of $O_2$ into the headspace. After equilibration, 250 $\mu$L of each headspace was injected into a gas chromatograph coupled to an isotope ratio mass spectrometer (GC/IRMS). The GC/IRMS instrument parameters and

procedures for determining concentrations of dissolved $O_2$, substrates, and products are described in Section S2.

$O_2$ consumption kinetics were determined in enzyme assays of identical composition but smaller volumes (2 mL) in completely filled crimp vials. Initial concentrations amounted to 1000 $\mu$M (nitro)aromatic substrates, 160–250 $\mu$M dissolved $O_2$ (obtained from mixing with $O_2$-free buffer), 100 $\mu$M $(NH_4)_2Fe(SO_4)_2$, and 1000 $\mu$M of NADH. Dissolved $O_2$ concentrations were monitored continuously with an optical oxygen microsensor (PreSens - Precision Sensing GmbH), which was introduced into closed crimp vials through a stainless-steel needle.

$H_2O_2$ formation was qualitatively probed in the 11 mL enzyme assays described above with nitrobenzene or 2-nitrophenol as substrates (Section S2.3). The reaction was initiated through the addition of 250 $\mu$M NADH, and $O_2$ consumption was monitored continuously thereafter (Figure S1). After 9–11 min reaction time (corresponding to approx. 40% $O_2$ turnover), 3.5 mg of catalase (100 $\mu$L of a 35 mg/mL stock solution) was added. An increase in $O_2$ concentration after catalase addition was interpreted as a qualitative indication of the presence of $H_2O_2$. Additionally, we used a quantitative assay for $H_2O_2$ formation based on the horseradish peroxidase (HRP)-catalyzed scavenging of $H_2O_2$ with concomitant oxidation of aniline. This assay was conducted in a 2 mL filled crimp vial as described above containing 200 $\mu$M nitrobenzene, 100 $\mu$M $(NH_4)_2Fe(SO_4)_2$, 600 $\mu$M aniline, and 10 mg/L HRP. Concentrations of nitrobenzene, aniline, and $NO_2^-$ were determined before the addition of NADH (500 $\mu$M initial concentration) and after 20 min. We assumed immediate, HRP-catalyzed oxidation of aniline and reduction of $H_2O_2$ to water and calculated the total amount of $H_2O_2$ released from NBDO from the decrease in aniline concentration. The latter was referenced with an external calibration row of aniline consumption by HRP within a $H_2O_2$ concentration range of 0–450 $\mu$M in the assay (Figure S2).

Initial rates of nitrite formation were determined in experiments with nitrobenzene, 3-nitrotoluene, 2,6-dinitrotoluene, 2-, 3-, and 4-fluoronitrobenzene, and 2-, 3-, and 4-chloronitrobenzene at 10 different initial substrate concentrations ranging from 10 $\mu$M to 300 $\mu$M. Experiments were performed at approximately 25 °C in 2 mL plastic tubes containing 0.3 $\mu$M oxygenase, 3.6 $\mu$M ferredoxin, 0.3 $\mu$M reductase, 500 $\mu$M $(NH_4)_2Fe(SO_4)_2$, and 500 $\mu$M NADH in MES buffer. After initiation of the reaction through addition of aqueous substrate stock solution, 300 $\mu$L samples were withdrawn every 10 s. The reaction was quenched with 300 $\mu$L of sulfanilamide (10 g $L^{-1}$ in 1.5 M HCl) followed by quantification of nitrite as described in Section S2.

**Chemical and Isotopic Analyses.** Procedures used for the quantification of aqueous concentrations of nitrated and hydroxylated aromatic compounds, $O_2$, $NO_2^-$, and NADH as well as $^{18}O/^{16}O$ and $^{13}C/^{12}C$ ratios of $O_2$ and nitroaromatic substrates follow principles introduced by Pati et al.[90] as described in Section S2.

**Data Evaluation.** *Reaction Kinetics.* The kinetics of initial $O_2$ consumption and nitrite formation in the presence of different substrates $i$ were evaluated in separate assays (see above) during periods of linear concentration changes vs time from linear regressions. Initial rates of $O_2$ consumption, $\nu_{0, O_2}^i$, were determined from continuous measurements of dissolved $O_2$ concentration, $c_{O_2}$, during the first 2–6 min (Figures S3 and

S10–S13). Initial rates of nitrite formation, $\nu_{0, NO_2^-}^i$, were obtained from repeated sampling during the first 120 s after substrate addition (Figure S14).

Maximum rates ($\nu_{max}^i$) and Michaelis constants ($K_m^i$) of nitrite formation in the presence of different substrates $i$ were determined with a non-linear least square regression according to eq 1

$$\nu_{0,NO_2^-}^i = \frac{\nu_{max}^i \cdot c_0^i}{K_m^i + c_0^i} = \frac{k_{cat}^i \cdot E_0 \cdot c_0^i}{K_m^i + c_0^i} \quad (1)$$

where $\nu_{0, NO_2^-}^i$ is the initial rate of $NO_2^-$ formation from substrate $i$, $c_0^i$ is the nominal initial substrate concentration, $k_{cat}^i$ is the observable first-order rate constant, and $E_0$ is the nominal concentration of active sites in NBDO, corresponding to 3 mol per mol of oxygenase. By contrast, $\nu_{max}^i$ and $K_m^i$ for $O_2$ consumption were obtained from the continuous measurement of $O_2$ concentration ($c_{O_2}$) over time in a single assay. The rate of $O_2$ consumption at each time-point ($\nu_{O_2}^i$) was calculated as the derivative of measured $c_{O_2}$ vs time (i.e., $\Delta[O_2]/\Delta t$). We used non-linear least square regression according to eq S2 with the derived $\nu_{O_2}^i$ and measured $c_{O_2}^i$ values to estimate $\nu_{max}^i$ and $K_m^i$.

All reported parameter values for $\nu_{max}^i$, $k_{cat}^i$, and $K_m^i$ were corrected for the specific activity of the oxygenase component used in each experiment, which was determined from nitrite formation kinetics with 200 $\mu$M nitrobenzene ($\nu_0^{ref} = 0.51$ $\mu$M $NO_2^-$ $s^{-1}$). Linear and nonlinear regression analyses were performed with Igor Pro software (WaveMetrics, Inc.), and all parameter uncertainties are reported as 95% confidence intervals.

Reaction stoichiometries of substrate dioxygenation and $O_2$ consumption were derived on the basis of the generalized nitroarene dioxygenation by NBDO (Scheme 1) and normalized to the amount of external reduction equivalents (NADH).

**Scheme 1. Dioxygenation of Substituted Nitroarenes to Catechol and Nitrite Catalyzed by Nitrobenzene Dioxygenase (NBDO)**
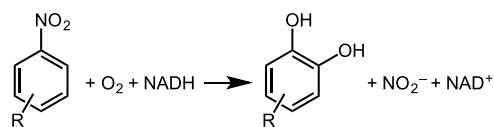


To that end, stoichiometric coefficients of species $j$, $|\nu_j|$, were calculated on the basis of 5 to 8 experimental replicates through linear regressions of eq 2 where different concentrations of nitroaromatic substrate, dissolved $O_2$, hydroxylated aromatic product, and $NO_2^-$ were obtained by limiting the amount of added NADH

$$[j] = \nu_j \cdot [NADH] + b \quad (2)$$

where $[j]$ stands for the measured molar concentration changes of substrates, dissolved $O_2$, hydroxylated organic product, and nitrite at the end of an experiment, respectively, [NADH] is the nominal concentration of NADH, and $b$ is the $y$-intercept (Figure S4). Uncertainties in $|\nu_j|$ reflect errors that arise from linear regression analysis weighted with 2% standard deviation of measurement uncertainty and are reported as 95%

confidence intervals. The extent of $O_2$ uncoupling, $f_{O_2-uc}$, was calculated through linear regressions of eq 3 from the molar concentration of $NO_2^-$, $[NO_2^-]$, and the amount of $O_2$ consumed in three to five replicate experiments

$$[NO_2^-] = (1 - f_{O_2-uc}) \cdot ([O_2]_0 - [O_2]) + b \tag{3}$$

where $[O_2]_0$ and $[O_2]$ are the dissolved $O_2$ concentrations at the beginning and end of an experiment, respectively.

*Isotope Effects.* Kinetic isotope effects averaging over both O atoms in $O_2$ ($^{18}$O-KIE) were calculated as in previous studies on the $O_2$ activation of various enzymes[86,87,94−96] through non-linear least square regression of data from samples with different degrees of $O_2$ consumption as in eq 4

$$\frac{^{18}R_{corr}}{^{18}R_0} = \left(\frac{[O_2]}{[O_2]_0}\right)^{1/^{18}O\text{-}KIE-1} \tag{4}$$

where $^{18}R_{corr}$ is the blank-corrected $^{18}O/^{16}O$ ratio of $O_2$ in a sample after complete NADH oxidation and $^{18}R_0$ is the isotope ratio of a NADH-free sample without $O_2$ consumption (i.e., $[O_2]/[O_2]_0 = 1$). Kinetic isotope effects of aromatic carbon hydroxylation ($^{13}$C-KIE) in the substrate were derived accordingly for nitroaromatic compounds as in eq 5

$$\frac{^{13}R_{corr}}{^{13}R_0} = \left(\frac{[S]}{[S]_0}\right)^{(1/(n \cdot (^{13}C\text{-}KIE-1))} \tag{5}$$

where $^{13}R_{corr}$ is the $^{13}C/^{12}C$ ratio of the substrate in a sample after partial conversion, $^{13}R_0$ is the isotope ratio of an unreacted substrate, and $[S]$ is the substrate concentration. $n$ stands for the number of carbon atoms in the substrate and accounts for the "dilution" of the isotope effect according to the assumption of an asynchronous dioxygenation mechanism.[50,90]

## RESULTS AND DISCUSSION

**Substrate-Specific Oxygen Activation Rates of Nitrobenzene Dioxygenase.** Initial rates of $O_2$ activation by NBDO for a broad range of substrates were obtained under steady-state conditions from continuous measurement of dissolved $O_2$ in enzyme assays that contained no headspace and are compiled in Table S1. Concentration trends from experiments with selected substrates are shown in Figure 1. We identified three types of substrate-dependent NBDO behaviors. First, previously identified substrates for NBDO including nitrobenzene and mono- and dinitrotoluenes caused $O_2$ consumption at 5−90 $\mu$M min$^{-1}$ (Table S1). These substrates as well as the halogenated nitrobenzenes tested herein led to complete $O_2$ removal within 10 min and generation of the hydroxylation products, $NO_2^-$ and (substituted) catechols, as shown previously.[97−99] The initial rates of $O_2$ consumption in the absence of substrates and reduction equivalents (NADH) were more than 50-fold slower and only increased slightly in the presence of NADH (1.8 ± 0.1 $\mu$M s$^{-1}$, Table S1 and Figure S3). These observations agree with previous studies, which showed that activation of $O_2$ by Rieske dioxygenases requires the presence of a substrate in the active site.[45,52,100−102] Second, benzoate a substrate for other Rieske dioxygenases,[22,49] was unreactive in the presence of NBDO and did not lead to $O_2$ activation that exceeded the rates observed in blank experiments. The same observation was made with other substrates, such as pentachloronitrobenzene and benzene.
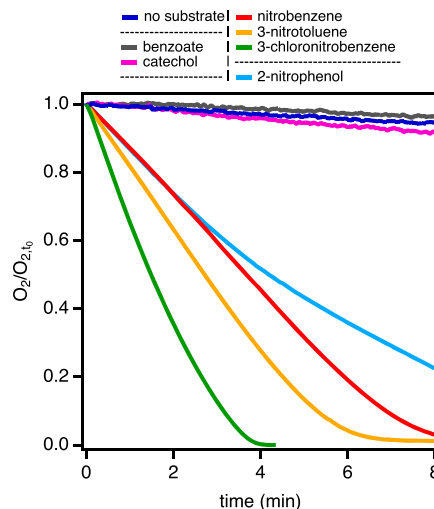


**Figure 1.** Normalized decrease of dissolved $O_2$ concentrations in headspace-free enzyme assays containing NBDO, NADH, and selected substrates according to the three types of substrate-dependent observations (see Table S1 for the complete list of evaluated substrates).

Third, substrates such as 2-nitrophenol caused $O_2$ activation at similar initial rates and extents to (substituted) nitrobenzenes and nitrotoluenes (Figure 1) but did not cause measurable substrate transformation (see below).

**Substrate-Specific Ratios of Substrate Dihydroxylation to Oxygen Activation.** Mass balances of substrates and $O_2$ turnover and reaction stochiometries were determined at different extents of conversion by limiting the concentration of external reduction equivalents (NADH) in the assays. Figure 2 exemplarily shows the increasing consumption of nitrobenzene and dissolved $O_2$ with increasing nominal concentrations of NADH in the assays. Nitrobenzene was transformed stoichiometrically to equal amounts of catechol and $NO_2^-$ (Scheme 1) and the sum of nitrobenzene and either catechol or $NO_2^-$ concentration corresponded to the initial substrate concen-
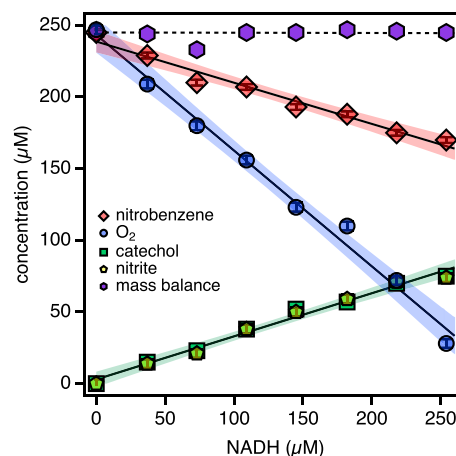


**Figure 2.** Nitrobenzene, dissolved $O_2$, catechol, $NO_2^-$ concentrations, and the mass balance of nitrobenzene and catechol concentrations in NBDO assays after complete consumption of different amounts of NADH. The slope of the black lines and the shaded areas represent $v_j$ values and their 95% confidence intervals of the regression with eq 2, respectively, and the corresponding data are shown in Table 1 and Table S2.

**Table 1. Stoichiometries for O$_2$ Activation and Dioxygenation of 10 Substituted Nitrobenzenes by NBDO as well as the $^{13}$C-KIE and $^{18}$O-KIE Values of the Substrates$^a$**

| entry | (co)substrate | $v_j$[b] | $f_{O_2\text{-uc}}$[c] | $^{18}$O-KIE | $^{13}$C-KIE |
|---|---|---|---|---|---|
| 1a | nitrobenzene | 0.32 ± 0.01 | 0.67 ± 0.01 | | 1.023 ± 0.001[d] |
| 1b | O$_2$ (NB) | 0.78 ± 0.01 | | 1.016 ± 0.001 | |
| 2a | 3-nitrotoluene | 0.68 ± 0.02 | 0.31 ± 0.02 | | 1.003 ± 0.001[d] |
| 2b | O$_2$ (3-NT) | 1.01 ± 0.01 | | 1.015 ± 0.003 | |
| 3a | 2,6-dinitrotoluene | 0.48 ± 0.02 | 0.57 ± 0.01 | | 1.008 ± 0.003[d] |
| 3b | O$_2$ (2,6-DNT) | 0.98 ± 0.01 | | 1.016 ± 0.001 | |
| 4a | 2-fluoronitrobenzene | 0.35 ± 0.01 | 0.60 ± 0.01 | | 1.020 ± 0.003 |
| 4b | O$_2$ (2-F-NB) | 0.84 ± 0.01 | | 1.016 ± 0.005 | |
| 5a | 3-fluoronitrobenzene | 0.59 ± 0.02 | 0.41 ± 0.02 | | 1.004 ± 0.004 |
| 5b | O$_2$ (3-F-NB) | 0.92 ± 0.01 | | 1.016 ± 0.006 | |
| 6a | 4-fluoronitrobenzene | 0.28 ± 0.01 | 0.70 ± 0.01 | | 1.035 ± 0.002 |
| 6b | O$_2$ (4-F-NB) | 0.78 ± 0.01 | | 1.018 ± 0.005 | |
| 7a | 2-chloronitrobenzene | 0.35 ± 0.01 | 0.64 ± 0.01 | | 1.020 ± 0.006 |
| 7b | O$_2$ (2-Cl-NB) | 0.80 ± 0.01 | | 1.017 ± 0.006 | |
| 8a | 3-chloronitrobenzene | 0.74 ± 0.02 | 0.27 ± 0.02 | | 0.999 ± 0.003 |
| 8b | O$_2$ (3-Cl-NB) | 0.94 ± 0.01 | | 1.014 ± 0.005 | |
| 9a | 4-chloronitrobenzene | 0.24 ± 0.01 | 0.74 ± 0.01 | | 1.021 ± 0.001 |
| 9b | O$_2$ (4-Cl-NB) | 0.74 ± 0.01 | | 1.016 ± 0.002 | |
| 10 | O$_2$ (2-NP) | 0.99 ± 0.01 | 1[e] | 1.019 ± 0.001 | n.a.[f] |

$^a$Uncertainties correspond to 95% confidence intervals. $^b$NADH-normalized stoichiometry of (co)substrate consumption calculated with eq 2; substrate dihydroxylation is quantified on the basis of measured NO$_2^-$ concentrations. $^c$O$_2$ uncoupling determined with eq 3. $^d$Reproduced from Pati et al.[91] $^e$Equation 3, no NO$_2^-$ observed. $^f$n.a. not applicable.

tration. This mass balance confirmed the absence of any other nitrobenzene transformation products.

The stoichiometric coefficients for substrates and O$_2$ consumption, $v_j$, which were normalized to the amount of added NADH (eq 2), are summarized in Table 1 and Table S2. In the presence of nitrobenzene, O$_2$ consumption by NBDO per amount of added NADH was close to stoichiometric (0.78 ± 0.01 mol of O$_2$/mol of NADH, Table 1, entry 1b), suggesting a nearly complete electron transfer from NADH to the terminal oxygenase via the reductase and ferredoxin. The stoichiometric coefficients of nitrobenzene consumption as well as NO$_2^-$ and catechol formation amounted to only 0.3 mol/mol NADH and are identical within uncertainty (Table 1 and Table S2). These numbers illustrate the consistent quantification of reaction products of nitroarene oxygenation by NBDO. For comparison with earlier works,[40,90] we henceforth used NO$_2^-$ concentrations for quantification of substrate hydroxylation and O$_2$ uncoupling. Entries 1a/b in Table 1 show that in the presence of nitrobenzene, only 35% of the activated O$_2$ is utilized for substrate dihydroxylation, whereas the remaining 65% reflects unproductive activation of O$_2$ ($f_{O_2\text{-uc}}$). Kinetic examination of NBDO-catalyzed nitrobenzene dioxygenation and O$_2$ consumption confirms the observation of O$_2$ uncoupling. $k_{cat}$ values for substrate dihydroxylation are approximately half of those derived for O$_2$ consumption (see $k_{cat}^S$ and $k_{cat}^{O_2}$ in Table S3). The O$_2$ uncoupling quantified with eq S3 on the basis of $k_{cat}$-ratios was 59 ± 4% and thus identical within uncertainty to the $f_{O_2\text{-uc}}$ values presented in Table 1.

Similar observations were made with NBDO assays containing eight alternative substrates, namely, two nitrotoluenes as well as three fluorinated and three chlorinated nitrobenzenes (Section S4.3, Figures S4a/b). O$_2$ consumption per NADH in the presence of either one of these substrates was close to stoichiometric as shown by $v_j$ values between 0.74

± 0.01 and 1.01 ± 0.01 (Table 1). The extents of substrate consumption and formation of the corresponding dioxygenation products on a NADH-normalized basis were substantially smaller. In NBDO assays with 3-nitrotoluene, 0.68 mol of nitrite was formed per mol of NADH added (Table 1, entry 2a) compared to only 0.24 in assays with 4-chloronitrobenzene (entry 9a). These results show that the substrate-specific efficiency of dioxygenation by NBDO ranged from 30 to 70%. Consistent with the lack of any observable disappearance of 2-nitrophenol in NBDO assays, we did not detect any NO$_2^-$ or hydroxylated products in such assays while O$_2$ uncoupling was stoichiometric.

**Evidence for Unproductive Activation of O$_2$ by NBDO.** O$_2$ uncoupling has been detected previously for other Rieske dioxygenases including NDO,[68,69] dibenzofuran dioxygenase,[66] and biphenyl dioxygenase.[65]

A comparison of O$_2$ uncoupling among these studies, however, can be difficult unless changes of substrates, products, and O$_2$ concentrations are referenced to NADH turnover and thus to the efficiency of electron transfer within the multicomponent enzyme system. In fact, O$_2$ can be consumed in the absence of the oxygenase component in reactions of NADH with the reductase and ferredoxin, especially in assays with overstoichiometric amounts of NADH.[65,103] This may lead to an overestimation of O$_2$ uncoupling. Here, we show that O$_2$ was not consumed in assays containing all components of the NBDO system except the substrate (Figure S3) and we explicitly normalize substrate turnover to the amount of NADH supplied (eq 2). Our estimates for O$_2$ uncoupling therefore reflect oxygenase activity (Table 1 and Tables S2 and S3).

Using a catalase-amended assay (Section S2.3), we observed that O$_2$ uncoupling in the presence of the substrates nitrobenzene and 2-nitrophenol coincided with the formation of H$_2$O$_2$ (Figure S1). The amount of H$_2$O$_2$ quantified through its horseradish peroxidase-catalyzed consumption in assays of

NBDO with nitrobenzene corresponded to 61% of $O_2$ consumption (Figure S5). This number matched the $O_2$ uncoupling quantified as $f_{O_2\text{-uc}}$ (0.67 ± 0.01, entry 1 in Table 1) within uncertainty and showed that $H_2O_2$ was the primary product of unproductive $O_2$ activation by NBDO. $H_2O_2$ is indeed the only $O_2$ uncoupling product reported so far for Rieske dioxygenases.[65,68,69] By contrast, the unproductive $O_2$ activation of substrate-chelating and cosubstrate-dependent non-heme $Fe^{II}$ oxygenases such as extradiol dioxygenases and 2-oxoglutarate-dependent oxygenases was associated with more diverse outcomes including generation of $H_2O_2$[103] and $O_2^{\bullet-}$,[104] complete oxygen reduction to $H_2O$,[105] and enzyme self-hydroxylation of tyrosine and tryptophan residues.[72−74]

It is generally hypothesized that $O_2$ uncoupling is caused by interferences of non-ideally bound substrates with the elementary reactions leading to $O_2$ activation, namely, loss of a $H_2O$ ligand from 6-coordinate non-heme $Fe^{II}$ and $O_2$ binding.[34,103,105] By contrast, $O_2$ uncoupling does not seem to alter the identity of the activated Fe-oxygen species. The good match between the amount of $O_2$ uncoupling and the detected $H_2O_2$ for nitrobenzene dioxygenation by NBDO suggests an $O_2$ activation as Fe-peroxo species. Imbeault et al.[65] speculated that the extent of $O_2$ uncoupling in biphenyl dioxygenase also leads to a decrease in $k_{cat}/K_m$ for $O_2$ with increasing $O_2$ uncoupling. While our $(k_{cat}/K_m)_{O_2}$ values (Table S3) vary within one order of magnitude for different substrates, no such trend with $O_2$ uncoupling was observed.

## $^{18}$O Kinetic Isotope Effects and Rate-Determining Steps of $O_2$ Activation.

Competitive $^{18}$O kinetic isotope effects ($^{18}$O-KIEs) on $k_{cat}/K_m$ of $O_2$ were determined from changes of the residual $^{18}$O/$^{16}$O in $O_2$ in the assays with all substrates. The similar $^{18}$O enrichment in $O_2$ (Figure S6) implies confinement of $^{18}$O-KIE values to a range between 1.014 and 1.019 (Table 1). These numbers illustrate an almost identical path to $O_2$ activation by NBDO in the presence of nitrobenzene, as well as methylated and halogenated substrates, and 2-nitrophenol.

Competitive $^{18}$O-KIEs have been introduced as probes for oxygen bonding changes from $O_2$ binding to a metal center up to and including the rate-determining step of $O_2$ activation.[88,89,106−109] Comparisons of $O_2$ activating processes among different non-heme $Fe^{II}$ oxygenases on the basis of $^{18}$O-KIE values exist,[85−87,110] albeit without consideration of Rieske dioxygenases due to the lack of data. This methodology is based on an evaluation of the magnitude of $^{18}$O-KIE against calculated $^{18}$O equilibrium isotope effects ($^{18}$O-EIEs), which serve as estimates for the upper limit for experimental $^{18}$O-KIE.[86−89,110−112] Calculated $^{18}$O-EIEs for $Fe^{III}$−$OO^{\bullet-}$ (1.0080), $Fe^{III}$−OOH (1.0172), and $Fe^{IV}$=O (1.0287) and other Fe-oxygen species[86] serve as benchmarks for $^{18}$O-KIEs and offer a means to infer the Fe-oxygen species involved in the rate-limiting steps of $O_2$ activation. Our $^{18}$O-KIEs for NBDO match $^{18}$O-EIEs for $Fe^{III}$−OOH quite closely while consistently exceeding those for $Fe^{III}$−$OO^{\bullet-}$ species. Figure 3a shows that the $^{18}$O-KIE values for substrates undergoing some degree of dioxygenation are identical within uncertainty and can be considered constant and substrate-independent. An average $^{18}$O-KIE of 1.016 would point to a rate-determining $O_2$ activation as $Fe^{III}$−OOH species. Observation of $H_2O_2$ as the stoichiometric product of $O_2$ uncoupling in the presence of nitrobenzene (Figure S5) corroborates this interpretation. The current view of the mechanisms of Rieske dioxygenases[50,51]
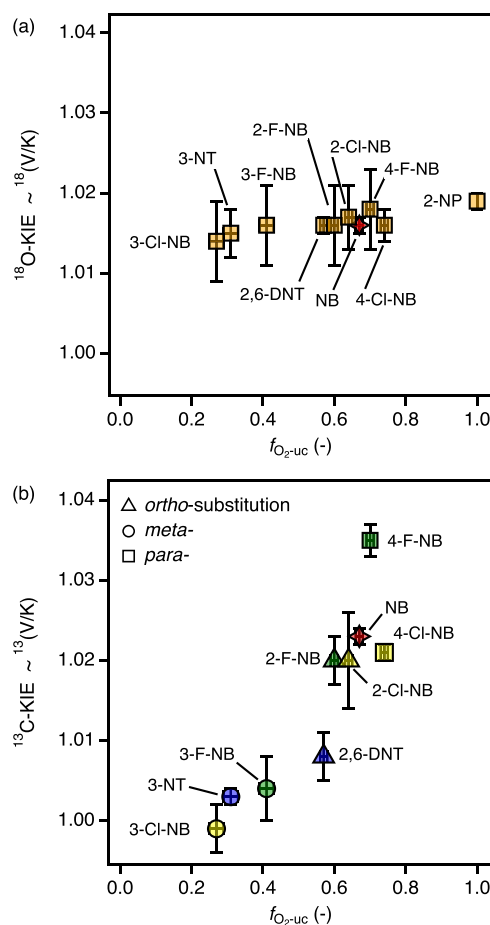


**Figure 3.** (a) $^{18}$O Kinetic isotope effects on $k_{cat}/K_m$ of $O_2$, also denoted as $^{18}(V/K)$, for $O_2$ activation by NBDO vs the fraction of $O_2$ uncoupling, $f_{O_2\text{-uc}}$, for the various nitroaromatic substrates. (b) $^{13}$C-KIEs of substrate dioxygenation vs $f_{O_2\text{-uc}}$. $^{13}$C-KIEs for nitrobenzene and nitrotoluenes are reproduced from Pati et al.[91] Error bars are 95% confidence intervals.

supports a substrate-independent $^{18}$O-KIE, describing the path to $O_2$ activation. In contrast to (co)substrate binding non-heme $Fe^{II}$ oxygenases where H atom transfer from the co-substrate is often a prerequisite of formation of high-valent Fe-$O_2$ species for substrate hydroxylation,[85,86,103,110] $O_2$ activation by Rieske dioxygenases does not entail any interaction of the substrate with the reactive Fe center.

Recent studies with BZDO suggest that Rieske dioxygenases react through $Fe^{III}$−$OO^{\bullet-}$ species followed by a fast proton coupled electron transfer from the reduced Rieske cluster to an $Fe^{III}$-peroxo-bridged substrate radical intermediate.[50,51] The $^{18}$O-KIE values of 1.016 presented herein, by contrast, would imply that the rate-determining step of $O_2$ activation in NBDO leads to $Fe^{III}$-peroxo intermediates. Formation of this species requires Rieske cluster oxidation prior to generation of species capable of substrate hydroxylation, and this pathway has been associated with $O_2$ activation by NDO.[57,113]

**Timing of Substrate Hydroxylation.** We probed for the timing of $O_2$ uncoupling in the catalytic cycle of NBDO by comparing the extent of $O_2$ uncoupling with the $^{13}$C-KIEs on $k_{cat}/K_m$ for the hydroxylation of nitrobenzene, nitrotoluenes, and halogenated nitrobenzenes (Table 1). $^{13}$C-KIE values of substrate dioxygenation were determined through the same methodology applied for the derivation of $^{18}$O-KIEs from

**Scheme 2. Catalytic Cycle of NBDO Exemplified with Nitrobenzene as the Substrate[a]**
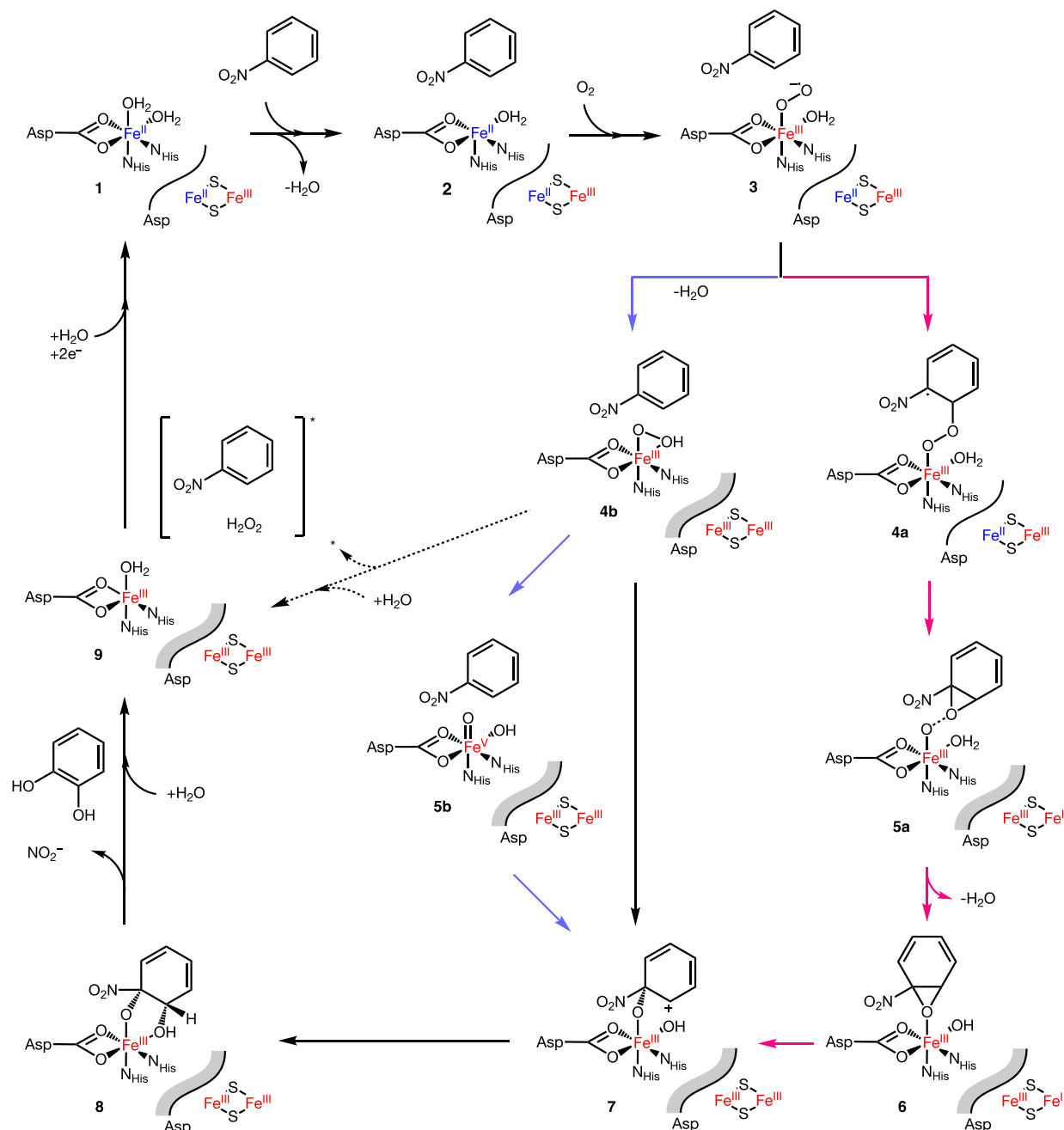


[a]The postulated contributions of $O_2$ uncoupling (dashed arrows) and concomitant release of unreacted substrate and $H_2O_2$ are shown in brackets. The BZDO-based mechanisms of $O_2$ activation (red arrows) corresponds to substrate attack by $Fe^{III}-OO^{\bullet-}$ through reaction path $3 \rightarrow 4a \rightarrow 5a \rightarrow 6$. The mechanism reported for NDO (light blue arrows) proceeds through reactions $3 \rightarrow 4b \rightarrow 5b \rightarrow 7$.[49−51] Gray shaded areas indicate the conformational shift of the mononuclear iron upon electron transfer from the Rieske cluster. Fe-oxygen species are shown based on studies with BZDO, NDO, and NBDO.[49,50,58] Species **7** is shown with the initial hydroxylation at $C_1$ in analogy to recent studies with benzoate in BZDO,[50] whereas Pabis et al.[58] propose this step to happen at $C_2$ for NBDO.

changes of residual $^{13}C$ in the aromatic substrate and in the dihydroxylated products.[90,91,114,115] The data in Table 1 (entries 1a to 9a) show that even though NBDO catalyzes the same reaction with exclusive formation of dihydroxylated aromatic products and $NO_2^-$ (Scheme 1 and Figure S4), $^{13}C$-KIE values varied substantially (i.e., between 0.999 and 1.035). The largest $^{13}C$-KIE found with 4-fluoronitrobenzene as the substrate agrees within uncertainty with the theoretical intrinsic $^{13}C$-KIEs for hydroxylations of the $C_2$ position of

nitrobenzene (1.038) calculated on the basis of asynchronous dioxygenation by high-valent $Fe^V$-oxo-hydroxo species ($5b \rightarrow 7 \rightarrow 8$, Scheme 2).[58,114] The involved $Fe^V=O(OH)$ species have been associated with the mechanisms of $O_2$ activation pertinent to NDO, which were obtained from experiments with $H_2O_2$ ("peroxide shunt mechanism").[50,51,59] Based on recent suggestions for Rieske dioxygenases made with BZDO,[49−51] however, experiments with dissolved $O_2$ (instead of $H_2O_2$) should proceed according to a mechanism in which

the substrate is attacked by $Fe^{III}-OO^{\bullet-}$ ($3 \rightarrow 4a \rightarrow 5a$, Scheme 2), leading to the formation of an $Fe^{III}$ epoxide species (6). This path has been referred to as the "native $O_2$ mechanism".[50] No intrinsic $^{13}C$-KIEs for substrate hydroxylation by Rieske dioxygenases in this mechanistic scenario are available, but data for transition states of alkene epoxidation[116] suggest that a magnitude of substrate isotope effects for formation of an epoxide intermediate 5a from hydroxylation by $Fe^{III}-OO^{\bullet-}$ would be between 1.012 and 1.023.

Our observation of a substrate $^{13}C$-KIE as large as 1.035 implies that the hydroxylation of the aromatic substrate is rate-determining in the catalytic cycle of NBDO. This interpretation apparently contradicts the notion of the rate-determining role of $O_2$ activation in non-heme $Fe^{II}$ oxygenases, which also follows from the observation of significant $^{18}O$-KIE on $k_{cat}/K_m(O_2)$ (Figure 3a). Conversely, the close to negligible $^{13}C$-KIE of 3-nitrotoluene and 3-fluoro- and 3-chloronitrobenzene near unity (0.999 to 1.004) would be consistent with the suggested kinetic mechanisms of Rieske dioxygenases[50,51,56,57] in that isotope effects of hydroxylation should be completely masked by the preceding formation of reactive Fe-oxygen species.

We also observe substituent effects on $f_{O_2\text{-uc}}$ and $^{13}C$-KIE values as well as on the correlation thereof (Figure 3b), which are difficult to rationalize, for example, as deactivation of the $C_2$ carbon of the substrate for electrophilic attack by Fe-oxygen species.[49,51] Methyl-, fluoro-, and chloro-substitution in the *meta* position is accompanied by a substantial reduction of both $O_2$ uncoupling and $^{13}C$-KIE-values compared to nitrobenzene. The clustering of these $f_{O_2\text{-uc}}$ and $^{13}C$-KIE values implies that electronic effects are not responsible for the observed correlation. By contrast, substituent effects are largely absent for most *ortho*- and *para*-substituted compounds. 2-F-, 2-Cl-, and 4-Cl-substituted nitrobenzenes exhibit almost identical $f_{O_2\text{-uc}}$ and $^{13}C$-KIE values to nitrobenzene. Finally, our data reveal a monotonic increase in $^{13}C$-KIE with the extent of $O_2$ uncoupling for fluoronitrobenzenes, but no so such trend was found for chlorinated compounds.

**Catalytic Cycle of NBDO.** We posit that $O_2$ uncoupling is associated with release of the apparently unreacted substrate. The uncoupling event allows for observation of substrate hydroxylation kinetics, a process that happens after the rate-limiting step(s) of the catalytic cycle of NBDO. Our interpretation is illustrated with the catalytic cycle in Scheme 2. For NBDO, the isotope-sensitive substrate hydroxylation steps can be part of both the BZDO- and NDO-based mechanisms and include reactions that would be $3 \rightarrow 4a \rightarrow 5a$ and $4b/5b/6 \rightarrow 7 \rightarrow 8$. Reactions leading from the resting state of NBDO (1) to reactive Fe-oxygen species 3, 4b, and 5b are considered rate-limiting.[50,56,58] Because the presence of substrates in the active site is a prerequisite for $O_2$ activation, these steps also determine the kinetics of substrate disappearance and thus should mask any $^{13}C$-KIEs pertinent to hydroxylation reactions. Measurement of substantial changes in $^{13}C/^{12}C$ ratios in the substrate in solution (Figures S7 and S8) therefore requires that some of the hydroxylation steps leading to catechol alter the $^{13}C/^{12}C$ ratios of the substrate prior to its release from the active site upon $O_2$ uncoupling.

Comparison of the reaction coordinate calculated for the $O_2$ activation mechanisms for NDO ($3 \rightarrow 4b \rightarrow 5b \rightarrow 7$)[57,58] and BDZO ($3 \rightarrow 4a \rightarrow 5a \rightarrow 6$)[50] and the fact that the substrate is

released in seemingly unreacted form suggest that the NDO-related mechanism shown in the central part of Scheme 2 is predominating in NBDO. Reaction coordinates for $5b \rightleftharpoons 7 \rightarrow 8$ and analyses of commitment factors from theoretical $^{13}C$-KIEs of NBDO[91] reveal that barrier heights for the stepwise hydroxylations up to the transition state between 7 and 8 are moderately small and close to 10 kcal mol$^{-1}$. Formation of 8, however, is exergonic by more than 40 kcal mol$^{-1}$.[50,58] This second hydroxylation step is thus irreversible for the substrate. These data imply that the reversible formation of singly hydroxylated nitroaromatic intermediate 7 and further reaction up to the transition state leading to 8 are plausible sources of the observed carbon isotope fractionation in the substrate if uncoupling is considered. From the perspective of the observed $^{13}C$-KIEs of the substrates, $O_2$ uncoupling and release of seemingly unreacted substrate after rate-limiting $O_2$ activation can thus occur from species 4b and 5b. The quantitative detection of $H_2O_2$ together with the assumption of an irreversible O–O bond cleavage[88] associated with the formation of 5b, however, implies that uncoupling occurs from 4b. It also follows from this scenario that the hydroxylation of the aromatic substrate by NBDO happens as $4b \rightarrow 7$ and thus does not go through $Fe^V$-oxo-hydroxo species 5b that have been proposed for NDO-based mechanisms. We postulate that the notable effects of aromatic substituents on both $f_{O_2\text{-uc}}$ and $^{13}C$-KIEs shown in Figure 3b affect the ability of NBDO to keep the substrate aligned in the active site for the first hydroxylation step $4b \rightarrow 7$, an argument that has been invoked for explaining the uncoupling of $O_2$ activation and substrate hydroxylation by $\alpha$-ketoglutarate-dependent oxygenases.[80] *Meta*-substitution appears to favor this reaction compared to all other nitroaromatic substrates. Moreover, $^{18}O$ KIE-based evidence for rate-limiting $Fe^{III}-OOH$ formation exclude $O_2$ uncoupling from Fe-superoxo species 3. We also exclude the release of unreacted substrate from 3 prior to $H_2O_2$ formation through electron transfer from the Rieske cluster (Figure S9). In fact, several previous observations imply that Rieske cluster oxidation requires the presence of substrates in the active site.[45,49,53]

Hydroxylation steps of the BZDO-based mechanism include species 4a, 5a, and 6. While the initial step of substrate hydroxylation in reaction $3 \rightarrow 4a$ could, in principle, give rise to substrate isotope fractionation, several points make this scenario unlikely. First, the formation of 4a is followed by the highly exergonic proton-coupled electron transfer from the Rieske cluster $4a \rightarrow 5a$.[50] This reaction is likely to mask any substrate isotope effect on $3 \rightarrow 4a$ through forward commitment to catalysis.[117] Second, this mechanism cannot lead to the observed $O_2$ uncoupling with the release of seemingly unreacted substrate. Uncoupling during reaction $3 \rightarrow 4a$ would again require the unlikely Rieske cluster oxidation in the absence of substrates for the release of $H_2O_2$ (Figure S9). Third, the release of nitroepoxide-like intermediates from 5a and 6 prior to the second hydroxylation step ($6 \rightarrow 7 \rightarrow 8$) implies that one of the two oxygen atoms of $O_2$ would have been used in a monooxygenation reaction as reported for other Rieske dioxygenases.[118,119] $O_2$ activation would then no longer be uncoupled. Hydrolysis of the nitroepoxide intermediate[120] followed by reduction of the cyclic hydroxyketone product can generate catechol (Figure S10). This process would make the release of a nitroepoxide intermediate from the active site indistinguishable from substrate dioxygenation in our experiments. We conclude that the observation of substrate carbon

isotope fractionation and $O_2$ uncoupling would not be compatible with a reaction through the BZDO-based catalytic mechanism.

The catalytic cycle for NBDO in Scheme 2 also offers two additional, alternative interpretations for reconciliation of the different ^{13}C-KIEs observed for the various NBDO substrates. These options, however, contradict other aspects of the above hypotheses. The first one would be to postulate substrate-dependent rate-determining steps in the NBDO catalytic cycle. The highest ^{13}C-KIEs could be seen as evidence for rate-determining hydroxylation for 4-fluoronitrobenzene (**4b → 7**) by NBDO, whereas any of the steps involved in $O_2$ activation (i.e., **2 → 3 → 4b(→ 5b)**) would be the kinetic bottleneck for reactions with *meta*-substituted nitrobenzenes. Such catalytic scenarios have been reported for other oxygenases where large intrinsic substrate oxygenation ^{13}C-KIEs of 1.05 can be almost completely masked through rate-limiting $O_2$ activation,[92] but it would leave the systematic extent of $O_2$ uncoupling observed here for NBDO in Figure 3b unexplained.

The second option would be that the substrates react through a combination of NDO- and BZDO-based mechanisms and that this ratio is, again, substrate-dependent. Nitrobenzene as well as 2-/4-fluoro- and 2-/4-chloronitrobenzenes would be dioxygenated predominantly through the catalytic mechanism proposed for NDO, which exhibits $O_2$ uncoupling whereas 3-nitrotoluene, 3-fluoro-, and 3-chloronitrobenzene would react primarily through the BZDO mechanism where neither $O_2$ uncoupling nor substrate carbon isotope fractionation could happen. This combination of reaction pathways could explain different substrate ^{13}C-KIEs but would require different ^{18}O-KIEs for $O_2$ activation for the substrates such as smaller ^{18}O-KIEs with *meta*-substituted nitrobenzenes as substrates. Our ^{18}O-KIE data do not agree with this interpretation. Substrate-dependent mechanisms would also contradict the implicit assumptions of a common aromatic hydroxylation path for Rieske dioxygenases made throughout the literature.[15,16,18,20,25,42,113]

## CONCLUSIONS

Our work shows that accounting for $O_2$ uncoupling in the catalytic cycle of Rieske dioxygenases allows for rationalizing seemingly contrasting observations on enzyme reactivity toward a broad range of substrates. While $O_2$ activation is the rate-limiting step of catalysis that happens without direct interaction of the substrate with the non-heme $Fe^{II}$ center, aromatic substrate transformation nevertheless reveals compound-specific reaction kinetics. The observation of substrate hydroxylation isotope effects of very different magnitude can be reconciled by considering the equally compound-specific release of unreacted substrate upon $O_2$ uncoupling. Despite evidence for the role of substrate fit in the active site from substituent effects, it is currently quite speculative to explain the magnitude of $O_2$ uncoupling. We hypothesize that the electronic properties of the substrate bound in the active site pocket could exert some allosteric control on $O_2$ activation and thus also be responsible for the efficiency of hydroxylation. We found recently for another Rieske dioxygenase that the electron affinity of the substrate bound in the active site can modulate the thermodynamics of the metal-to-substrate charge transfer from the Rieske cluster through the $H_2O$ ligand prior to coordination changes at the non-heme $Fe^{II}$.[46] Because the presence of the substrate is accompanied by conformational changes that allow for $O_2$ activation at the non-heme Fe, we envision that these processes lead to an orientation of the substrate toward reactive Fe-oxygen species that favors hydroxylation. We note that the proposed catalytic cycle that includes $O_2$ uncoupling is compatible with mechanisms of NDO but not with the one proposed for BZDO. The observation of distinct catalytic cycles for Rieske dioxygenases warrants further study on the $O_2$ uncoupling. Finally, this work allows postulating a mechanistic basis for assessing the activity of Rieske dioxygenases toward xenobiotic compounds in the environment, the generation of reactive oxygen species, and the ensuing enzymatic adaptation to new substrates.

## ■ ASSOCIATED CONTENT

### ⓢ Supporting Information

The Supporting Information is available free of charge at https://pubs.acs.org/doi/10.1021/acscatal.2c00383.

Chemicals and biological materials used, method descriptions for chemical and isotopic analyses, and additional reaction schemes, figures, and tables on enzyme kinetics, reaction stoichiometries, and carbon and oxygen isotope fractionation (PDF)

## ■ AUTHOR INFORMATION

### Corresponding Author

**Thomas B. Hofstetter** − *Eawag, Swiss Federal Institute of Aquatic Science and Technology, 8600 Dübendorf, Switzerland; Institute of Biogeochemistry and Pollutant Dynamics (IBP), ETH Zürich, 8092 Zürich, Switzerland;* ⓞ orcid.org/0000-0003-1906-367X; Phone: +41 58 765 50 76; Email: thomas.hofstetter@eawag.ch; Fax: +41 58 765 50 28

### Authors

**Sarah G. Pati** − *Eawag, Swiss Federal Institute of Aquatic Science and Technology, 8600 Dübendorf, Switzerland; Institute of Biogeochemistry and Pollutant Dynamics (IBP), ETH Zürich, 8092 Zürich, Switzerland;* Present Address: Department of Environmental Sciences, University of Basel, 4056 Basel, Switzerland; ⓞ orcid.org/0000-0001-8170-4074

**Charlotte E. Bopp** − *Eawag, Swiss Federal Institute of Aquatic Science and Technology, 8600 Dübendorf, Switzerland; Institute of Biogeochemistry and Pollutant Dynamics (IBP), ETH Zürich, 8092 Zürich, Switzerland*

**Hans-Peter E. Kohler** − *Eawag, Swiss Federal Institute of Aquatic Science and Technology, 8600 Dübendorf, Switzerland*

Complete contact information is available at:
https://pubs.acs.org/10.1021/acscatal.2c00383

### Author Contributions

§S.G.P. and C.E.B. contributed equally to this work.

### Notes

The authors declare no competing financial interest.

## ■ REFERENCES

(1) Barry, S. M.; Challis, G. L. Mechanism and catalytic diversity of Rieske non-heme iron-dependent oxygenases. *ACS Catal.* **2013**, *3*, 2362−2370.

(2) Withall, D.; Haynes, S.; Challis, G. Stereochemistry and mechanism of undecylprodigiosin oxidative carbocyclization to Streptorubin B by the Rieske oxygenase RedG. *J. Am. Chem. Soc.* **2015**, *137*, 7889−7897.

(3) Lukowski, A.; Ellinwood, D.; Hinze, M.; DeLuca, R.; Du Bois, J.; Hall, S.; Narayan, A. C−H Hydroxylation in paralytic shellfish toxin biosynthesis. *J. Am. Chem. Soc.* **2018**, *140*, 11863−11869.

(4) Ferraro, D. J.; Gakhar, L.; Ramaswamy, S. Rieske business: Structure-function of Rieske non-heme oxygenases. *Biochem. Biophys. Res. Commun.* **2005**, *338*, 175−190.

(5) Sydor, P. K.; Barry, S. M.; Odulate, O. M.; Barona-Gomez, F.; Haynes, S. W.; Corre, C.; Song, L.; Challis, G. L. Regio- and stereodivergent antibiotic oxidative carbocyclizations catalysed by Rieske oxygenase-like enzymes. *Nat. Chem.* **2011**, *3*, 388−392.

(6) Perry, C.; de Los Santos, E.; Alkhalaf, L.; Challis, G. Rieske non-heme iron-dependent oxygenases catalyse diverse reactions in natural product biosynthesis. *Nat. Prod. Rep.* **2018**, *35*, 622−632.

(7) Chen, Q.; Wang, C. H.; Deng, S. K.; Wu, Y.-D.; Li, Y.; Yao, L.; Jiang, J. D.; Yan, X.; He, J.; Li, S. P. Novel three-component Rieske non-heme iron oxygenase system catalyzing the *N*-dealkylation of chloroacetanilide herbicides in sphingomonads DC-6 and DC-2. *Appl. Environ. Microbiol.* **2014**, *80*, 5078−5085.

(8) Dumitru, R.; Jiang, W. Z.; Weeks, D. P.; Wilson, M. A. Crystal structure of dicamba monooxygenase: A Rieske nonheme oxygenase that catalyzes oxidative demethylation. *J. Mol. Biol.* **2009**, *392*, 498−510.

(9) D'Ordine, R. L.; Rydel, T. J.; Storek, M. J.; Sturman, E. J.; Moshiri, F.; Bartlett, R. K.; Brown, G. R.; Eilers, R. J.; Dart, C.; Qi, Y.; Flasinski, S.; Franklin, S. J. Dicamba monooxygenase: Structural insights into a dynamic Rieske oxygenase that catalyzes an exocyclic monooxygenation. *J. Mol. Biol.* **2009**, *392*, 481−497.

(10) Jiang, W.; Wilson, M. A.; Weeks, D. P. O-Demethylations catalyzed by Rieske nonheme iron monooxygenases involve the difficult oxidation of a saturated C—H Bond. *ACS Chem. Biol.* **2013**, *8*, 1687−1691.

(11) Schuster, J.; Schafer, F.; Hubler, N.; Brandt, A.; Rosell, M.; Hartig, C.; Harms, H.; Muller, R. H.; Rohwerder, T. Bacterial degradation of *tert*-amyl alcohol proceeds via hemiterpene 2-methyl-3-buten-2-ol by employing the tertiary alcohol desaturase function of the Rieske nonheme mononuclear iron oxygenase MdpJ. *J. Bacteriol.* **2012**, *194*, 972−981.

(12) Dunham, N. P.; Arnold, F. H. Nature's machinery, repurposed: Expanding the repertoire of iron-dependent oxygenases. *ACS Catal.* **2020**, *10*, 12239−12255.

(13) Münch, J.; Püllmann, P.; Zhang, W.; Weissenborn, M. J. Enzymatic hydroxylations of sp³-carbons. *ACS Catal.* **2021**, *11*, 9168−9203.

(14) Solomon, E. I.; Brunold, T. C.; Davis, M. I.; Kemsley, J. N.; Lee, S. K.; Lehnert, N.; Neese, F.; Skulan, A. J.; Yang, Y. S.; Zhou, J. Geometric and electronic structure/function correlations in non-heme iron enzymes. *Chem. Rev.* **2000**, *100*, 235−350.

(15) Solomon, E. I.; Light, K. M.; Liu, L. V.; Srnec, M.; Wong, S. D. Geometric and electronic structure contributions to function in non-heme iron enzymes. *Acc. Chem. Res.* **2013**, *46*, 2725−2739.

(16) Solomon, E. I.; Goudarzi, S.; Sutherlin, K. D. O₂ activation by non-heme iron enzymes. *Biochemistry* **2016**, *55*, 6363−6374.

(17) Costas, M.; Mehn, M.; Jensen, M.; Que, L. Dioxygen activation at mononuclear nonheme iron active sites: Enzymes, models, and intermediates. *Chem. Rev.* **2004**, *104*, 939−986.

(18) Kal, S.; Que, L. Dioxygen activation by nonheme iron enzymes with the 2-His-1-carboxylate facial triad that generate high-valent oxoiron oxidants. *J. Biol. Inorg. Chem.* **2017**, *22*, 339−365.

(19) Bollinger, J. M., Jr.; Krebs, C. Enzymatic C−H activation by metal−superoxo intermediates. *Curr. Opin. Chem. Biol.* **2007**, *11*, 151−158.

(20) Bruijnincx, P. C. A.; van Koten, G.; Klein Gebbink, R. J. M. Mononuclear non-heme iron enzymes with the 2-His-1-carboxylate facial triad: recent developments in enzymology and modeling studies. *Chem. Soc. Rev.* **2008**, *37*, 2716−2744.

(21) Kovaleva, E. G.; Neibergall, M. B.; Chakrabarty, S.; Lipscomb, J. D. Finding intermediates in the O₂ activation pathways of non-heme iron oxygenases. *Acc. Chem. Res.* **2007**, *40*, 475−483.

(22) Kovaleva, E. G.; Lipscomb, J. D. Versatility of biological non-heme Fe(II) centers in oxygen activation reactions. *Nat. Chem. Biol.* **2008**, *4*, 186−193.

(23) Krebs, C.; Fujimori, D. G.; Walsh, C. T.; Bollinger, J. M., Jr.; J Martin Bollinger, J. Non-heme Fe(IV)-oxo intermediates. *Acc. Chem. Res.* **2007**, *40*, 484−492.

(24) Islam, M. S.; Leissing, T. M.; Chowdhury, R.; Hopkinson, R. J.; Schofield, C. J. 2-Oxoglutarate-dependent oxygenases. *Annu. Rev. Biochem.* **2018**, *87*, 585−620.

(25) Bugg, T. D. H.; Ramaswamy, S. Non-heme iron-dependent dioxygenases: unravelling catalytic mechanisms for complex enzymatic oxidations. *Curr. Opin. Chem. Biol.* **2008**, *12*, 134−140.

(26) Boyd, D.; Bugg, T. Arene *cis*-dihydrodiol formation: from biology to application. *Organ. Biomol. Chem.* **2006**, *4*, 181−192.

(27) Sutherlin, K. D.; et al. Nuclear resonance vibrational spectroscopy definition of O₂ intermediates in an extradiol dioxygenase: Correlation to crystallography and reactivity. *J. Am. Chem. Soc.* **2018**, *140*, 16495−16513.

(28) Davis, M.; Wasinger, E.; Decker, A.; Pau, M.; Vaillancourt, F.; Bolin, J.; Eltis, L.; Hedman, B.; Hodgson, K.; Solomon, E. I. Spectroscopic and electronic structure studies of 2,3-dihydroxybiphenyl 1,2-dioxygenase: O₂ Reactivity of the non-heme ferrous site in extradiol dioxygenases. *J. Am. Chem. Soc.* **2003**, *125*, 11214−11227.

(29) Peck, S. C.; Wang, C.; Dassama, L. M.; Zhang, B.; Guo, Y.; Rajakovich, L. J.; Bollinger, J. M., Jr.; Krebs, C.; Van Der Donk, W. A. O−H activation by an unexpected ferryl intermediate during catalysis by 2-hydroxyethylphosphonate dioxygenase. *J. Am. Chem. Soc.* **2017**, *139*, 2045−2052.

(30) Peck, S. C.; Chekan, J. R.; Ulrich, E. C.; Nair, S. K.; Van Der Donk, W. A. A common late-stage intermediate in catalysis by 2-hydroxyethyl-phosphonate dioxygenase and methylphosphonate synthase. *J. Am. Chem. Soc.* **2015**, *137*, 3217−3220.

(31) Knoot, C. J.; Purpero, V. M.; Lipscomb, J. D. Crystal structures of alkylperoxo and anhydride intermediates in an intradiol ring-cleaving dioxygenase. *Proc. Natl. Acad. Sci. U. S. A.* **2015**, *112*, 388−393.

(32) Vaillancourt, F. H.; Bolin, J. T.; Eltis, L. D. The ins and outs of ring-cleaving dioxygenases. *Crit. Rev. Biochem. Mol. Biol.* **2006**, *41*, 241−267.

(33) Pau, M. Y. M.; Davis, M. I.; Orville, A. M.; Lipscomb, J. D.; Solomon, E. I. Spectroscopic and electronic structure study of the enzyme-substrate complex of intradiol dioxygenases: Substrate activation by a high-spin ferric non-heme iron site. *J. Am. Chem. Soc.* **2007**, *129*, 1944−1958.

(34) Iyer, S. R.; Chaplin, V. D.; Knapp, M. J.; Solomon, E. I. O₂ activation by nonheme Fe^II α-ketoglutarate-dependent enzyme variants: Elucidating the role of the facial triad carboxylate in FIH. *J. Am. Chem. Soc.* **2018**, *140*, 11777−11783.

(35) Eser, B. E.; Barr, E. W.; Frantorn, P. A.; Saleh, L.; Bollinger, J. M., Jr.; Krebs, C.; Fitzpatrick, P. F. Direct spectroscopic evidence for a high-spin Fe(IV) intermediate in tyrosine hydroxylase. *J. Am. Chem. Soc.* **2007**, *129*, 11334−11335.

(36) Kauppi, B.; Lee, K.; Carredano, E.; Parales, R. E.; Gibson, D. T.; Eklund, H.; Ramaswamy, S. Structure of an aromatic-ring-hydroxylating dioxygenase-naphthalene 1,2-dioxygenase. *Structure* **1998**, *6*, 571−586.

(37) Karlsson, A.; Parales, J. V.; Parales, R. E.; Gibson, D. T.; Eklund, H.; Ramaswamy, S. Crystal structure of naphthalene dioxygenase: Side-on binding of dioxygen to iron. *Science* **2003**, *299*, 1039−1042.

(38) Nojiri, H.; Ashikawa, Y.; Noguchi, H.; Nam, J.-W.; Urata, M.; Fujimoto, Z.; Uchimura, H.; Terada, T.; Nakamura, S.; Shimizu, K.;

Yoshida, T.; Habe, H.; Omori, T. Structure of the terminal oxygenase component of angular dioxygenase, carbazole 1,9a-dioxygenase. *J. Mol. Biol.* **2005**, *351*, 355−370.

(39) Furusawa, Y.; Nagarajan, V.; Tanokura, M.; Masai, E.; Fukuda, M.; Senda, T. Crystal structure of the terminal oxygenase component of biphenyl dioxygenase derived from *Rhodococcus* sp. Strain RHA1. *J. Mol. Biol.* **2004**, *342*, 1041−1052.

(40) Friemann, R.; Ivkovic-Jensen, M. M.; Lessner, D. J.; Yu, C. L.; Gibson, D. T.; Parales, R. E.; Eklund, H.; Ramaswamy, S. Structural insight into the dioxygenation of nitroarene compounds: the crystal structure of nitrobenzene dioxygenase. *J. Mol. Biol.* **2005**, *348*, 1139−1151.

(41) Parales, R. E.; Parales, J. V.; Gibson, D. T. Aspartate 205 in the catalytic domain of naphthalene dioxygenase is essential for activity. *J. Bacteriol.* **1999**, *181*, 1831−1837.

(42) Gibson, D. T.; Parales, R. E. Aromatic hydrocarbon dioxygenases in environmental biotechnology. *Curr. Opin. Biotech.* **2000**, *11*, 236−243.

(43) Resnick, S. M.; Gibson, D. T. Regio- and stereospecific oxidation of fluorene, dibenzofuran, and dibenzothiophene by naphthalene dioxygenase from *Pseudomonas* sp strain NCIB 9816-4. *Appl. Environ. Microbiol.* **1996**, *62*, 4073−4080.

(44) Inoue, K.; Ashikawa, Y.; Umeda, T.; Abo, M.; Katsuki, J.; Usami, Y.; Noguchi, H.; Fujimoto, Z.; Terada, T.; Yamane, H.; Nojiri, H. Specific interactions between the ferredoxin and terminal oxygenase components of a class IIB Rieske nonheme iron oxygenase, carbazole 1,9a-dioxygenase. *J. Mol. Biol.* **2009**, *392*, 436−451.

(45) Ohta, T.; Chakrabarty, S.; Lipscomb, J. D.; Solomon, E. I. Near-IR MCD of the non-heme ferrous active ste in naphthalene 1,2-dioxygenase: Correlation to crystallography and structural Insight into the mechanism of Rieske dioxygenases. *J. Am. Chem. Soc.* **2008**, *130*, 1601−1610.

(46) Csizi, K.-S.; Eckert, L.; Brunken, C.; Hofstetter, T. B.; Reiher, M. The apparently unreactive substrate facilitates the electron transfer for dioxygen activation in Rieske dioxygenases. *Chem. - Eur. J.* **2022**, *28*, No. e202103937.

(47) Carredano, E.; Karlsson, A.; Kauppi, B.; Choudhury, D.; Parales, R. E.; Parales, J. V.; Lee, K.; Gibson, D. T.; Eklund, H.; Ramaswamy, S. Substrate binding site of naphthalene 1,2-dioxygenase: Functional implications of indole binding. *J. Mol. Biol.* **2000**, *296*, 701−712.

(48) Koehntop, K. D.; Emerson, J. P.; Que, L. The 2-His-1-carboxylate facial triad: a versatile platform for dioxygen activation by mononuclear non-heme iron(II) enzymes. *J. Biol. Inorg. Chem.* **2005**, *10*, 87−93.

(49) Rivard, B. S.; Rogers, M. S.; Marell, D. J.; Neibergall, M. B.; Chakrabarty, S.; Cramer, C. J.; Lipscomb, J. D. Rate-determining attack on substrate precedes Rieske cluster oxidation during *cis*-dihydroxylation by benzoate dioxygenase. *Biochemistry* **2015**, *54*, 4652−4664.

(50) Sutherlin, K. D.; et al. NRVS Studies of the peroxide shunt intermediate in a Rieske dioxygenase and its relation to the native $Fe^{II}$ $O_2$ reaction. *J. Am. Chem. Soc.* **2018**, *140*, 5544−5559.

(51) Rogers, M. S.; Lipscomb, J. D. Salicylate 5-hydroxylase: Intermediates in aromatic hydroxylation by a Rieske monooxygenase. *Biochemistry* **2019**, *58*, 5305−5319.

(52) Wolfe, M. D.; Parales, J. V.; Gibson, D. T.; Lipscomb, J. D. Single turnover chemistry and regulation of $O_2$ activation by the oxygenase component of naphthalene 1,2-dioxygenase. *J. Biol. Chem.* **2001**, *276*, 1945−1953.

(53) Wolfe, M. D.; Altier, D. J.; Stubna, A.; Popescu, C. V.; Munck, E.; Lipscomb, J. D. Benzoate 1,2-dioxygenase from *Pseudomonas putida*: Single turnover kinetics and regulation of a two-component Rieske dioxygenase. *Biochemistry* **2002**, *41*, 9611−9626.

(54) Liu, L. V.; Hong, S.; Cho, J.; Nam, W.; Solomon, E. I. Comparison of high-spin and low-spin nonheme $Fe^{III}$-OOH complexes in O-O bond homolysis and H-atom abstraction reactivities. *J. Am. Chem. Soc.* **2013**, *135*, 3286−3299.

(55) Pabis, A.; Geronimo, I.; York, D. M.; Paneth, P. Molecular dynamics simulation of nitrobenzene dioxygenase using AMBER force field. *J. Chem. Theory Comput.* **2014**, *10*, 2246−2254.

(56) Bassan, A.; Blomberg, M. R. A.; Siegbahn, P. E. M. A theoretical study of the *cis*-dihydroxylation mechanism in naphthalene 1,2-dioxygenase. *J. Biol. Inorg. Chem.* **2004**, *9*, 439−452.

(57) Bassan, A.; Blomberg, M. R. A.; Borowski, T.; Siegbahn, P. E. M. Oxygen activation by Rieske non-heme iron oxygenases, a theoretical insight. *J. Phys. Chem. B* **2004**, *108*, 13031−13041.

(58) Pabis, A.; Geronimo, I.; Paneth, P. A DFT study of the *cis*-dihydroxylation of nitroaromatic compounds catalyzed by nitro-benzene dioxygenase. *J. Phys. Chem. B* **2014**, *118*, 3245−3256.

(59) Wolfe, M. D.; Lipscomb, J. D. Hydrogen peroxide-coupled *cis*-diol formation catalyzed by naphthalene 1,2-dioxygenase. *J. Biol. Chem.* **2003**, *278*, 829−835.

(60) Chakrabarty, S.; Austin, R. N.; Deng, D. Y.; Groves, J. T.; Lipscomb, J. D. Radical intermediates in monooxygenase reactions of Rieske dioxygenases. *J. Am. Chem. Soc.* **2007**, *129*, 3514−3515.

(61) Neibergall, M. B.; Stubna, A.; Mekmouche, Y.; Munck, E.; Lipscomb, J. D. Hydrogen peroxide dependent *cis*-dihydroxylation of benzoate by fully oxidized benzoate 1,2-dioxygenase. *Biochemistry* **2007**, *46*, 8004−8016.

(62) Wackett, L. P. Mechanism and applications of Rieske non-heme iron dioxygenases. *Enzyme Microb. Technol.* **2002**, *31*, 577−587.

(63) Resnick, S. M.; Lee, K.; Gibson, D. T. Diverse reactions catalyzed by naphthalene dioxygenase from *Pseudomonas* sp strain NCIB 9816. *J. Ind. Microbiol. Biotechnol.* **1996**, *17*, 438−457.

(64) Ferraro, D. J.; Okerlund, A. L.; Mowers, J. C.; Ramaswamy, S. Structural basis for regioselectivity and stereoselectivity of product formation by naphthalene 1,2-dioxygenase. *J. Bacteriol.* **2006**, *188*, 6986−6994.

(65) Imbeault, N. Y.; Powlowski, J. B.; Colbert, C. L.; Bolin, J. T.; Eltis, L. D. Steady-state kinetic characterization and crystallization of a polychlorinated biphenyl-transforming dioxygenase. *J. Biol. Chem.* **2000**, *275*, 12430−12437.

(66) Bünz, P. V.; Cook, A. M. Dibenzofuran 4, 4a-dioxygenase from *Sphingomonas* sp. strain RW1: angular dioxygenation by a three-component enzyme system. *J. Bacteriol.* **1993**, *175*, 6467−6475.

(67) Yang, T. C.; Wolfe, M. D.; Neibergall, M. B.; Mekmouche, Y.; Lipscomb, J. D.; Hoffman, B. M. Modulation of substrate binding to naphthalene 1,2-dioxygenase by Rieske cluster reduction/oxidation. *J. Am. Chem. Soc.* **2003**, *125*, 2034−2035.

(68) Lee, K.-S.; Gibson, D. T. Toluene and ethylbenzene oxidation by purified naphthalene dioxygenase from *Pseudomonas* sp. Strain NCIB 9816-4. *Appl. Environ. Microbiol.* **1996**, 3101−3106.

(69) Lee, K. Benzene-induced uncoupling of naphthalene dioxygenase activity and enzyme inactivation by production of hydrogen peroxide. *J. Bacteriol.* **1999**, *181*, 2719−2725.

(70) Yang, T. C.; Wolfe, M. D.; Neibergall, M. B.; Mekmouche, Y.; Lipscomb, J. D.; Hoffman, B. M. Substrate binding to NO-ferro-naphthalene 1,2-dioxygenase studied by high-resolution Q-band pulsed H-2-ENDOR spectroscopy. *J. Am. Chem. Soc.* **2003**, *125*, 7056−7066.

(71) Bopp, C. E.; Kohler, H.-P. E.; Hofstetter, T. B. Enzyme kinetics of organic contaminant oxygenations. *Chimia* **2020**, *74*, 108−114.

(72) Liu, A.; Ho, R.; Que, L.; Ryle, M.; Phinney, B.; Hausinger, R. Alternative reactivity of an $\alpha$-ketoglutarate-dependent iron(II) oxygenase: enzyme self-hydroxylation. *J. Am. Chem. Soc.* **2001**, *123*, 5126−5127.

(73) Liu, P.; Mehn, M.; Yan, F.; Zhao, Z.; Que, L.; Liu, H. Oxygenase activity in the self-hydroxylation of (*S*)-2-hydroxypropyl-phosphonic acid epoxidase involved in fosfomycin biosynthesis. *J. Am. Chem. Soc.* **2004**, *126*, 10306−10312.

(74) Mantri, M.; Zhang, Z.; McDonough, M.; Schofield, C. Autocatalysed oxidative modifications to 2-oxoglutarate dependent oxygenases. *FEBS J.* **2012**, *279*, 1563−1575.

(75) Gu, M.; Imlay, J. A. Superoxide poisons mononuclear iron enzymes by causing mismetallation. *Mol. Microbiol.* **2013**, *89*, 123−134.

(76) Imlay, J. A. The mismetallation of enzymes during oxidative stress. *J. Biol. Chem.* **2014**, *289*, 28121−28128.

(77) Müller, I.; Stückl, C.; Wakeley, J.; Kertesz, M.; Usón, I. Succinate complex crystal structures of the alpha-ketoglutarate-dependent dioxygenase AtsK: steric aspects of enzyme self-hydroxylation. *J. Biol. Chem.* **2005**, *280*, 5716−5723.

(78) Chen, Y.; Comeaux, L.; Eyles, S.; Knapp, M. Auto-hydroxylation of FIH-1: an Fe(II), $\alpha$-ketoglutarate-dependent human hypoxia sensor. *Chem. Commun.* **2008**, 4768−4770.

(79) Goudarzi, S.; Iyer, S.; Babicz, J.; Yan, J.; Peters, G.; Christensen, H.; Hedman, B.; Hodgson, K.; Solomon, E. Evaluation of a concerted vs. sequential oxygen activation mechanism in $\alpha$-ketoglutarate-dependent nonheme ferrous enzymes. *Proc. Natl. Acad. Sci. U. S. A.* **2020**, *117*, 5152−5159.

(80) McCusker, K. P.; Klinman, J. P. Modular behavior of tauD provides insight into the origin of specificity in $\alpha$-ketoglutarate-dependent nonheme iron oxygenases. *Proc. Natl. Acad. Sci.* **2009**, *106*, 19791−19795.

(81) McCusker, K. P.; Klinman, J. P. An active-site phenylalanine directs substrate binding and C-H cleavage in the $\alpha$-ketoglutarate-dependent dioxygenase TauD. *J. Am. Chem. Soc.* **2010**, *132*, 5114−5220.

(82) Nikel, P. I.; Fuhrer, T.; Chavarría, M.; Sánchez-Pascuala, A.; Sauer, U.; de Lorenzo, V. Reconfiguration of metabolic fluxes in *Pseudomonas putida* as a response to sub-lethal oxidative stress. *The ISME Journal* **2021**, *15*, 1751−1766.

(83) Pérez-Pantoja, D.; Nikel, P. I.; Chavarria, M.; de Lorenzo, V. Endogenous stress caused by faulty oxidation reactions fosters evolution of 2,4-dinitrotoluene-degrading bacteria. *PLoS Genet.* **2013**, *9*, e1003764−e1003711.

(84) Pérez-Pantoja, D.; Nikel, P. I.; Chavarría, M.; de Lorenzo, V. Transcriptional control of 2,4-dinitrotoluene degradation in Burkholderia sp. R34 bears a regulatory patch that eases pathway evolution. *Environ. Microbiol.* **2021**, *23*, 2522−2531.

(85) Zhu, H.; Peck, S. C.; Bonvin, F.; van der Donk, W. A.; Klinman, J. P. Oxygen-18 kinetic isotope effects of nonheme iron ezymes HEPD and MPnS support ron(III) superoxide as the hydrogen abstraction species. *J. Am. Chem. Soc.* **2015**, 10448−10451.

(86) Mirica, L. M.; McCusker, K. P.; Munos, J. W.; Liu, H.-w.; Klinman, J. P. $^{18}$O Kinetic isotope effects in non-heme iron enzymes: Probing the nature of Fe/O$_2$ intermediates. *J. Am. Chem. Soc.* **2008**, *130*, 8122−8123.

(87) Tian, G.; Klinman, J. Discrimination between $^{16}$O and $^{18}$O in oxygen-binding to the reversible oxygen carriers hemoglobin, myoglobin, hemerythrin, and hemocyanin - a new probe for oxygen-binding and reductive activation by proteins. *J. Am. Chem. Soc.* **1993**, *115*, 8891−8897.

(88) Roth, J. P.; Klinman, J. P. In *Isotope Effects in Chemistry and Biology*; Kohen, A., Limbach, H.-H., Eds.; CRC Press/Taylor & Francis: New York, 2006; pp 645−669, DOI: 10.1201/9781420028027.ch24.

(89) Lanci, M.; Roth, J. Oxygen isotope effects upon reversible O$_2$-binding reactions: Characterizing mononuclear superoxide and peroxide structures. *J. Am. Chem. Soc.* **2006**, *128*, 16006−16007.

(90) Pati, S. G.; Kohler, H.-P. E.; Hofstetter, T. B. Characterization of substrate, cosubstrate, and product isotope effects associated with enzymatic oxygenations of organic compounds based on compound-specific isotope analysis. In *Measurement and Analysis of Kinetic Isotope Effects*; Harris, M. E., Anderson, V. E., Eds.; Academic Press, 2017; pp. 292−329, DOI: 10.1016/bs.mie.2017.06.044.

(91) Pati, S. G.; Kohler, H.-P. E.; Pabis, A.; Paneth, P.; Parales, R. E.; Hofstetter, T. B. Substrate and enzyme specificity of the kinetic isotope effects associated with the dioxygenation of nitroaromatic contaminants. *Environ. Sci. Technol.* **2016**, *50*, 6708−6716.

(92) Wijker, R. S.; Pati, S. G.; Zeyer, J.; Hofstetter, T. B. Enzyme kinetics of different types of flavin-dependent monooxygenases determine the observable contaminant stable isotope fractionation. *Environ. Sci. Technol. Lett.* **2015**, *2*, 329−334.

(93) Pati, S. G.; Bolotin, J.; Brennwald, M. S.; Kohler, H.-P. E.; Werner, R. A.; Hofstetter, T. B. Measurement of oxygen isotope ratios ($^{18}$O/$^{16}$O) of aqueous O$_2$ in small samples by gas chromatography/isotope ratio mass spectrometry. *Rapid Commun. Mass Spectrom.* **2016**, *30*, 684−690.

(94) Purdy, M.; Koo, L.; de Montellano, P.; Klinman, J. Mechanism of O$_2$ activation by cytochrome P450cam studied by isotope effects and transient state kinetics. *Biochemistry* **2006**, *45*, 15793−15806.

(95) Stahl, S. S.; Francisco, W. A.; Merkx, M.; Klinman, J. P.; Lippard, S. J. Oxygen kinetic isotope effects in soluble methane monooxygenase. *J. Biol. Chem.* **2001**, *276*, 4549−4553.

(96) Roth, J. P.; Klinman, J. P. Catalysis of electron transfer during activation of O$_2$ by the flavoprotein glucose oxidase. *Proc. Natl. Acad. Sci.* **2003**, *100*, 62−67.

(97) Johnson, G. R.; Spain, J. C. Synthesis of substituted catechols using nitroarene dioxygenases. *Enzyme Microb. Technol.* **2006**, *38*, 142−147.

(98) Lessner, D. J.; Johnson, G. R.; Parales, R. E.; Spain, J. C.; Gibson, D. T. Molecular characterization and substrate specificity of nitrobenzene dioxygenase from *Comamonas* sp strain JS765. *Appl. Environ. Microbiol.* **2002**, *68*, 634−641.

(99) Ju, K.-S.; Parales, R. E. Application of nitroarene dioxygenases in the design of novel strains that degrade chloronitrobenzenes. *Microbial Biotechnology* **2009**, *2*, 241−252.

(100) Neidig, M. L.; Solomon, E. I. Structure−function correlations in oxygen activating non-heme iron enzymes. *Chem. Commun.* **2005**, 5843−5863.

(101) Pavel, E. G.; Martins, L. J.; Ellis, W. R., Jr.; Solomon, E. I. Magnetic circular dichroism studies of exogenous ligand and substrate binding to the non-heme ferrous active site in phthalate dioxygenase. *Chem. Biol.* **1994**, *1*, 173−183.

(102) Gassner, G. T.; Ballou, D. P.; Landrum, G. A.; Whittaker, J. W. Magnetic circular dichroism studies on the mononuclear ferrous active site of phthalate dioxygenase from *Pseudomonas cepacia* show a change of ligation state on substrate binding. *Biochemistry* **1993**, *32*, 4820−4825.

(103) Thrower, J.; Mirica, L. M.; McCusker, K. P.; Klinman, J. P. Mechanistic Investigations of 1-Aminocyclopropane 1-Carboxylic Acid Oxidase with Alternate Cyclic and Acyclic Substrates. *Biochemistry* **2006**, *45*, 13108−13117.

(104) Vaillancourt, F. H.; Labbe, G.; Drouin, N. M.; Fortin, P. D.; Eltis, L. D. The mechanism-based inactivation of 2,3-dihydroxybiphenyl 1,2-dioxygenase by catecholic substrates. *J. Biol. Chem.* **2002**, *277*, 2019−2027.

(105) Dix, T. A.; Benkovic, S. J. Mechanism of "uncoupled" tetrahydropterin oxidation by phenylalanine hydroxylase. *Biochemistry* **1985**, *24*, 5839−5846.

(106) Roth, J. P. Oxygen isotope effects as probes of electron transfer mechanisms and structures of activated O$_2$. *Acc. Chem. Res.* **2009**, *42*, 399−408.

(107) Roth, J. P. Advances in studying bioinorganic reactions mechanisms: isotopic probes of activated oxygen intermediates in metalloenzymes. *Curr. Opin. Chem. Biol.* **2007**, *11*, 142−150.

(108) Smirnov, V.; Roth, J. Evidence for Cu$^−$O2 intermediates in superoxide oxidations by biomimetic copper(II) complexes. *J. Am. Chem. Soc.* **2006**, *128*, 3683−3695.

(109) Lanci, M.; Smirnov, V.; Cramer, C.; Gauchenova, E.; Sundermeyer, J.; Roth, J. Isotopic probing of molecular oxygen activation at copper(I) sites. *J. Am. Chem. Soc.* **2007**, *129*, 14697−14709.

(110) Mirica, L. M.; Klinman, J. P. The nature of O$_2$ activation by the ethylene-forming enzyme 1-aminocyclopropane-1-carboxylic acid oxidase. *Proc. Natl. Acad. Sci.* **2008**, *105*, 1814−1819.

(111) Roth, J.; Cramer, C. Direct examination of H$_2$O$_2$ activation by a heme peroxidase. *J. Am. Chem. Soc.* **2008**, *130*, 7802−7803.

(112) Roth, J. P.; Wincek, R.; Nodet, G.; Edmondson, D. E.; McIntire, W. S.; Klinman, J. P. Oxygen isotope effects on electron transfer to O$_2$ probed using chemically modified flavins bound to glucose oxidase. *J. Am. Chem. Soc.* **2004**, *126*, 15120−15131.

(113) Blomberg, M. R. A.; Borowski, T.; Himo, F.; Liao, R.-Z.; Siegbahn, P. E. M. Quantum chemical studies of mechanisms for metalloenzymes. *Chem. Rev.* **2014**, *114*, 3601−3658.

(114) Pati, S. G.; Kohler, H.-P. E.; Bolotin, J.; Parales, R. E.; Hofstetter, T. B. Isotope Effects of Enzymatic Dioxygenation of Nitrobenzene and 2-Nitrotoluene by Nitrobenzene Dioxygenase. *Environ. Sci. Technol.* **2014**, *48*, 10750−10759.

(115) Hofstetter, T. B.; Spain, J. C.; Nishino, S. F.; Bolotin, J.; Schwarzenbach, R. P. Identifying competing aerobic nitrobenzene biodegradation pathways using compound-specific isotope analysis. *Environ. Sci. Technol.* **2008**, *42*, 4764−4770.

(116) Singleton, D. A.; Merrigan, S. R.; Liu, J.; Houk, K. Experimental geometry of the epoxidation transition state. *J. Am. Chem. Soc.* **1997**, *119*, 3385−3386.

(117) Northrop, D. B. The expression of isotope effects on enzyme-catalyzed reactions. *Annu. Rev. Biochem.* **1981**, *50*, 103−131.

(118) Wackett, L. P.; Kwart, L. D.; Gibson, D. T. Benzylic monooxygenation catalyzed by toluene dioxygenase from *Pseudomonas putida*. *Biochemistry* **1988**, *27*, 1360−1367.

(119) Robertson, J.; Spain, J.; Haddock, J.; Gibson, D. T. Oxidation of nitrotoluenes by toluene dioxygenase: evidence for a mono-oxygenase reaction. *Appl. Environ. Microbiol.* **1992**, *58*, 2643−2648.

(120) Newman, H.; Angier, R. The preparation and chemistry of α-nitroepoxides. *Tetrahedron* **1970**, *26*, 825−836.